The Solar Twin Planet Search

II. A Jupiter twin around a solar twin

M. Bedell[1]⋆, J. Meléndez[2], J. L. Bean[1], I. Ramírez[3], M. Asplund[4], A. Alves-Brito[5], L. Casagrande[4], S. Dreizler[6], T. Monroe[2], L. Spina[2], and M. Tucci Maia[2]

[1] Department of Astronomy and Astrophysics, University of Chicago, 5640 S. Ellis Ave, Chicago, IL 60637, USA
  e-mail: `mbedell@oddjob.uchicago.edu`
[2] Departamento de Astronomia do IAG/USP, Universidade de São Paulo, Rua do Matão 1226, Cidade Universitária, 05508-900 São Paulo, SP, Brazil
[3] McDonald Observatory and Department of Astronomy, University of Texas at Austin, USA
[4] Research School of Astronomy and Astrophysics, The Australian National University, Cotter Road, Weston, ACT 2611, Australia
[5] Instituto de Fisica, Universidade Federal do Rio Grande do Sul, Av. Bento Goncalves 9500, Porto Alegre, RS, Brazil
[6] Institut für Astrophysik, University of Göttingen, Germany

June 26, 2015

ABSTRACT

Context. With high-precision radial velocity surveys reaching a sufficiently long time baseline, the domain of long-period planet detections has recently opened up. The search for Jupiter-like planets is especially important if we wish to investigate the prevalence of solar system analogs, but their detection is complicated by the existence of stellar activity cycles on similar timescales. Radial velocity data with sufficient long-term instrumental precision and robust methods of diagnosing activity are crucial to the detection of extrasolar Jupiters.
Aims. Through our HARPS survey for planets around solar twin stars, we have identified a promising Jupiter twin candidate around the star HIP11915. We characterize this Keplerian signal and investigate its potential origins in stellar activity.
Methods. We carry out a Markov chain Monte Carlo (MCMC) analysis of the radial velocity data. To examine the signal's origin, we employ a variety of statistical tests using activity diagnostics such as the Ca II H&K lines and line asymmetry tracers.
Results. Our analysis indicates that HIP11915 hosts a Jupiter-mass planet with a 3600-day orbital period and low eccentricity. Although we cannot definitively rule out an activity cycle interpretation, we find that a planet interpretation is more likely based on a joint analysis of RV and activity index data.
Conclusions. The challenges of long-period radial velocity signals addressed in this planet are critical for the ongoing discovery of Jupiter-like exoplanets. If planetary in nature, the signal investigated here represents a very close analog to the solar system in terms of both Sun-like host star and Jupiter-like planet.

Key words. planetary systems – planets and satellites: detection – techniques: radial velocities

1. Introduction

As the search for new exoplanets with the radial velocity (RV) technique continues, our detection capabilities have increased dramatically in two dimensions: smaller signals, such as those induced by short-orbit terrestrial-mass planets, can now be found thanks to the increased precision of modern RV spectrographs, and longer-period signals can also be identified thanks to an ever-increasing time baseline of data collection. Both of these detection capabilities are critical if we wish to find planetary systems comparable to our own solar system.

At the cutting edge of long-period planet detection is the search for Jupiter analogs. In terms of signal size, Jupiter induces by far the largest radial velocity shift on the Sun of any planet and therefore should be the first planet detected in a twin of the solar system. However, the need for more than a decade of observational coverage with a consistently precise RV zero point complicates the process of discovering such a planet, as

does the possibility of stellar magnetic activity cycles inducing RV variations on a similar timescale (Saar & Donahue 1997).

In spite of these challenges, a number of Jupiter analog candidates have been discovered from long-duration planet surveys (see e.g. Vogt et al. 2000; Naef et al. 2003; Wright et al. 2007, 2008; Howard et al. 2010; Boisse et al. 2012; Marmier et al. 2013; Wittenmyer et al. 2014; Feng et al. 2015). These surveys also demonstrate the prevalence of solar-like magnetic activity cycles, which can manifest in the stellar radial velocities (Lovis et al. 2011; Zechmeister et al. 2013). These cycles can generally be traced by their influence on activity diagnostics such as the Ca II H & K lines (Baliunas et al. 1995) and asymmetries of the spectral cross-correlation function (Dravins 1985). With careful attention to these diagnostics, we can minimize the influence of activity cycles and recover planet signatures around cycling stars (Dumusque et al. 2011).

Over the last four years, we have been conducting an RV planet search with the HARPS spectrograph (Mayor et al. 2003) targeting a specific subset of 63 stars selected by the proximity of their fundamental parameters to those of the Sun ($T_{\rm eff}$ within ~100 K, $\log(g)$ within ~0.1 dex, and [Fe/H] within ~0.1 dex).

These solar twin stars offer a unique opportunity to determine their compositions at a precision as good as 2% (see e.g. Meléndez et al. 2009; Ramírez et al. 2009; Bedell et al. 2014). We aim to combine this high-precision chemical analysis with the m s^{-1}-level detection capabilities of HARPS to investigate the star-planet connection at an unprecedented level of detail.

In this paper we present our first detection from the planet search program: a Jupiter twin around the solar twin HIP11915. HIP11915 was previously established as a solar twin in Ramírez et al. (2014) based on its fundamental properties ($T_{\rm eff}$ = 5760 ± 4 K, log g = 4.46 ± 0.01, and [Fe/H] = -0.059 ± 0.004). Its age, estimated from isochrone fitting to be 4.0 ± 0.6 Gyr, is also in keeping with the solar value (Ramírez et al. 2014). HIP11915 is a bright (m_V = 8.6) star with relatively low activity (log(R'_{HK}) < -4.8), making it an excellent target for high-precision RV monitoring. Based on a Keplerian signal in our HARPS RVs, we determine the planet candidate's orbital parameters. We also investigate the influence of stellar activity on our RV measurements.

2. Data

All of the RV data used in this paper were obtained with the HARPS spectrograph on the ESO 3.6-m telescope at La Silla Observatory and were processed with the dedicated HARPS pipeline. Forty-three data points spanning a time range from October 2009 to January 2015 came from our HARPS large program dedicated to solar twin stars (program ID 188.C-0265). An additional 13 measurements were taken from the publicly available archive data and span a time range from October 2003 to November 2013 (program IDs 072.C-0488, 089.C-0732, 091.C-0034, 092.C-0721, and 183.C-0972).

For the 43 measurements taken through our program, the star was observed in high-accuracy mode with the ThAr lamp as a simultaneous reference source. Each observation used a 900-second exposure time to minimize potential RV noise from the five-minute p-mode oscillations of solar-type stars. To obtain a radial velocity measurement, we selected a binary mask based on the G2 spectral type for cross-correlation by the pipeline. Due to their generally high signal-to-noise ratios (median SNR over the spectral range on order of 100), the pipeline-produced RV error estimates were generally below 1 m s^{-1}. We expect the actual uncertainties to be somewhat higher due to stellar noise and potential undiagnosed instrumental effects. To account for these, we added the pipeline-estimated errors in quadrature with a baseline error level of 1 m s^{-1}, following Dumusque et al. (2011) and in accordance with the scatter in our own HARPS survey's quietest stars.

The 13 archive measurements have exposure times ranging from 120 to 900 seconds. All were taken in high-accuracy mode without a source on the simultaneous reference fiber, so that even the low SNR measurements are not in danger of spectral contamination by the simultaneous reference source. The data were processed by the pipeline and error estimates were modified by us as described above. An additional 1.1 m s^{-1} was added in quadrature to the errors on all exposures under 15 minutes, based on the expected p-mode signal for a solar twin (Bazot et al. 2011).

We analyzed all of the reduced HARPS spectra to measure the Ca II H&K activity indices S_{HK} and log(R'_{HK}) at each observation epoch. This was done according to the methods of Lovis et al. (2011). Errors on S_{HK} were estimated from photon noise.

Complete RV and S_{HK} data are available in Table 3, along with the HARPS pipeline-estimated activity indicators BIS and FWHM.

3. Analysis and Results

The RMS of the RVs is 6.5 m s^{-1}, indicating the presence of a signal stronger than the predicted stellar jitter of 2.1 m s^{-1} (Wright 2005). Visual inspection and a periodogram analysis of the data clearly show a long-period trend in the stellar radial velocities. We ran a grid search across a range of periods from 0 to 10,000 days and found the minimum chi-squared value lies near 3600 days.

We inspected the data for signs of stellar activity manifesting in the RVs. A strong correlation between radial velocity and the activity index S_{HK} is seen in the measurements from recent years, although there is no correlation in the archival data. Similar RV-correlated behavior is seen for other activity indicators including the bisector inverse slope (BIS), FWHM, V_{span}, and the biGaussian fit differential (as defined by Queloz et al. 2001; Boisse et al. 2011; Figueira et al. 2013). Doing a weighted linear least-squares fit and removing the trend with any of these activity indicators from the RVs results in reducing the correlations while preserving the long-period planet signal with high significance in a periodogram analysis. We additionally attempted the prescribed method of Dumusque et al. (2011) of fitting a long-period Keplerian to first an activity diagnostic and then (with period and phase fixed) the RVs. This method failed to remove the long-period power from the RVs regardless of whether S_{HK}, BIS, or FWHM was used as the diagnostic. The failure of these methods to successfully "clean" the data of its long-period signal suggests that the signal originates from a true Doppler shift rather than stellar activity, although activity is also present in the data.

3.1. Optimal Model: Keplerian Signal + S_{HK} Correlation

In the results presented here, we account for stellar activity by fitting a linear trend between RV and S_{HK} simultaneously with the Keplerian signal. This way the strength of the correlation between activity indicator and RV is free to change as the scatter induced by the Keplerian signal is removed. We use S_{HK} as the primary tracer of activity due to the unreliability of the BIS diagnostic for slow-rotating stars and the demonstrated efficiency of S_{HK} in removing activity cycle signals (Boisse et al. 2011; Meunier & Lagrange 2013). Other potential diagnostics and alternative model choices are explored in Section 3.2.

We ran a Markov chain Monte Carlo (MCMC) analysis to fit the radial velocity data to a model consisting of three components: a Keplerian signal, a linear correlation term with the S_{HK} values, and an offset term. This gives seven free parameters: the Keplerian parameters (P, K, e, ω + M_0, ω - M_0), where P is the orbital period, K is the RV semi-amplitude, e is eccentricity, ω is the argument of periastron, and M_0 is the mean anomaly at reference date t_0 = 2457000.0; a slope parameter α which relates the activity-induced change in RV to the corresponding change in S_{HK}; and an offset parameter, C. We additionally include an eighth free parameter, σ_J, representing the jitter which must be added in quadrature with the estimated RV error to make the measurement uncertainties consistent with the scatter in the residuals. This jitter physically corresponds to unknown Gaussian error which may arise from stellar noise or undiagnosed instrumental variations. When inputting the data, we subtracted a sigma-clipped median value from RV, S_{HK}, BIS, and FWHM for simplicity. This means that the offset parameter C is partially set by the difference between the median RV of the data set and the systemic RV of the star, but also includes the RV offset in the
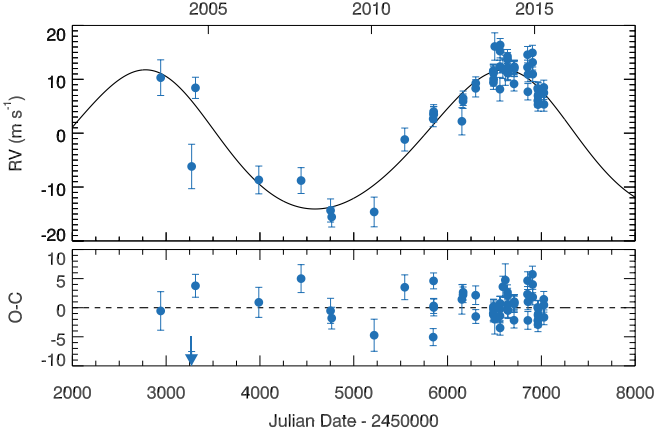
Fig. 1. Best-fit orbital solution for HIP11915b. Data points are the observed RVs with offset and S_{HK} correlation terms subtracted. One residual point is located outside of the plot range, as denoted by the arrow.

linear fit with the median-subtracted S_{HK} values (or any other correlations used in the model; see Section 3.2).

All of the fit parameters were given uniform priors except for P and K, which were sampled in log-space with a log-uniform prior. We ran five parallel chains and used the requirement of a Gelman-Rubin test statistic below 1.01 for all parameters to avoid non-convergence (Gelman & Rubin 1992). The best-fit orbital solution, plotted in Figure 1, corresponds to an approximately Jupiter-mass planet on a 10-year orbit with eccentricity consistent with zero (see Table 1). As seen in the MCMC posterior distributions (Figure 5), the chief source of uncertainty in the period measurement is in its degeneracy with eccentricity and the associated argument of periapse, parameters which are inevitably poorly constrained when only one orbit has been observed. The best-fit jitter term is consistent with the predicted stellar jitter of 2.1 m s^{-1} from the formula of Wright (2005).

After subtracting the best-fit planet signal, we searched for additional signals in the residuals with a generalized Lomb-Scargle periodogram analysis (Zechmeister & Kürster 2009). No significant periodicities were identified in the residuals to the planet fit or in the residuals to the planet and the fitted S_{HK} trend. We place constraints on the presence of additional planets in the system using a test based on the bootstrapping and injection of a planet signal into the residuals. For this test, we use the residuals to the planet fit only, and inflate the error bars (with jitter included) such that a flat-line fit to the residuals gives a reduced chi-squared of one. We then run a set of trials in which the RV data are resampled with replacement at the times of observation, a planet signal with period and semi-amplitude fixed and the other orbital parameters randomized is injected, and the reduced chi-squared of a flat-line fit to these simulated data is measured. If the chi-squared statistic has increased with three-sigma significance in 99 out of 100 trials at a given period and velocity semi-amplitude, we consider such a planet signal to be excluded based on its inconsistency with the scatter in the actual RVs. We run this trial until upper limits on planet presence are found for all of the periods in a log-sampled grid. The results rule out the presence of gas giants within a 1000-day orbital period, leaving open the possibility of inner terrestrial planets (Figure 2).

---

[1] **Error estimates do not include uncertainties on the stellar parameters, which were taken from Ramírez et al. (2014).**

Table 1. Best-fit parameters and uncertainties for HIP11915b.

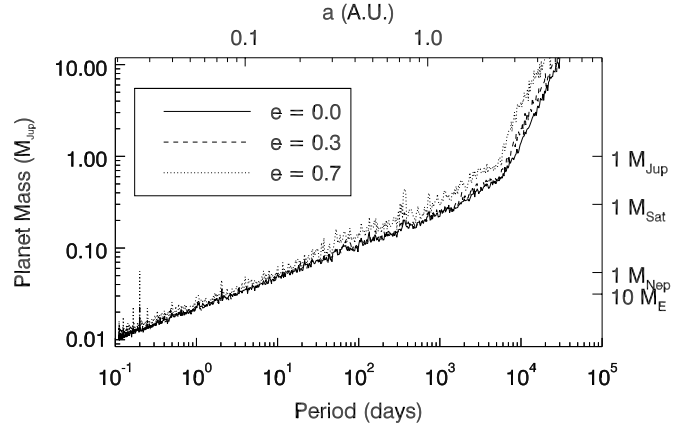| Parameter		Value	Uncertainty
P	[days]	3830	150
K	[m s^{-1}]	12.9	0.8
e		0.10	0.07
$\omega + M_0$	[rad]	3.0	1.3
$\omega - M_0$	[rad]	2.4	0.1
α	[m s^{-1} (unit S_{HK})$^{-1}$]	160	60
C	[m s^{-1}]	-11.0	1.3
σ_J	[m s^{-1}]	1.8	0.4
$m_p \sin(i)$	[M$_{Jup}$]	0.99	0.06 [1]
a	[AU]	4.8	0.1 [1]
RMS	[m s^{-1}]	2.9	

Fig. 2. Exclusion limits on potential planets in the RV data after subtraction of the 3600-day signal. Any signal in the parameter space located above the lines plotted would have induced a larger scatter in the RV residuals with three-sigma significance if present. Potential trends with activity indicators were not removed for this test to avoid underestimating the RV scatter.

3.2. Alternative Model Choices

It is not obvious from theory that the Keplerian + S_{HK} correlation model used above should be the best model choice. Other activity indicators exist and have been used with success to remove activity trends from RVs in the past. Chief among these are BIS and FWHM, both characteristics derived from the RV cross-correlation function (CCF) which measure the average spectral line asymmetry and/or broadening at the epoch of the observation (see e.g. Queloz et al. 2001, 2009). BIS or FWHM could potentially be used in place of S_{HK}. Also, because these indicators arise from distortions to the rotationally broadened stellar absorption lines while S_{HK} probes chromospheric emission, we could combine S_{HK} with a CCF-derived measurement to simultaneously track two separate physical indicators of activity.

We considered several alternative models before settling on the Keplerian + S_{HK} model as the best fit. A summary of models tried is given in Table 2. In all cases, the fitting was done with an MCMC as described above. The inclusion of a Keplerian signal is strongly justified, with the Keplerian + S_{HK} fit having a false alarm probability on order of 10^{-15} compared to the best fitting activity model (S_{HK} + FWHM). While the lowest χ^2 value is obtained for the fit to a Keplerian, S_{HK}, and FWHM, the addition of the FWHM term is not fully justified by the reduction in scatter

Table 2. Models considered.

Name	Degrees of Freedom	χ^2 of Fit
Keplerian only	50	162.54
Keplerian + S_{HK}	49	136.00
Keplerian + FWHM	49	145.32
Keplerian + BIS	49	133.96
Keplerian + S_{HK} + FWHM	48	129.50
S_{HK} only	54	897.78
BIS only	54	704.27
FWHM only	54	650.97
S_{HK} + BIS	53	719.28
S_{HK} + FWHM	53	639.76

around the fit. An F-test gives a formal false alarm probability of 13% for the Keplerian + S_{HK} + FWHM model compared to the simpler Keplerian + S_{HK} model. The Keplerian + S_{HK} fit has a false alarm probability of 0.3% when compared to the Keplerian only model. Using BIS in place of S_{HK} technically gives a slightly better fit, but we chose to use S_{HK} in the main analysis on grounds of BIS's previously noted unreliability for slow rotators. Regardless of the choice of activity indicator(s), all Keplerian fit parameters remain within the uncertainty intervals quoted in Table 1.

4. Planet or Activity Cycle?

The question of stellar activity's role in the observed radial velocities is of special importance given the proximity of the signal period to the 11-year solar magnetic cycle. The signal size is also consistent with the theoretically predicted 10-11 m s^{-1} signal for a solar activity cycle (Meunier & Lagrange 2013). However, an activity cycle should manifest not only in the observed RVs but also in other diagnostics. We expect a positive correlation in RV with the activity index S_{HK} as well as with other diagnostics such as BIS and the FWHM of the cross-correlation function (Lovis et al. 2011; Zechmeister et al. 2013). While such correlations are seen, they appear insufficient to fully explain the observed RVs.

For at least two other solar twins in our sample, similar Jupiter-like RV variations are seen; however, in these cases subtracting a linear fit with S_{HK} entirely removes the long-period power from a periodogram and reduces the RMS of RVs to a level consistent with the expected stellar jitter. In contrast, the RV signal inferred from the variation of S_{HK} or any other activity tracer for HIP11915 is much smaller in size than the total RV signal, so that significant power remains at long periods in the periodogram.

A large sample of stars with activity cycles have been studied with HARPS by Lovis et al. (2011), who derived empirical predictions for the expected correlation between RV and other activity indictors with R'_{HK} as a function of stellar temperature and metallicity. The correlations seen for HIP11915 are generally lower than the predicted values: $C_{RV} = 30 \pm 1$ m s^{-1} (unit R'_{HK})$^{-1}$, $C_{FWHM} = 58 \pm 2$ m s^{-1} (unit R'_{HK})$^{-1}$, and $C_{BIS} = 22.4 \pm 0.7$ m s^{-1} (unit R'_{HK})$^{-1}$ from their Equations 9-12, while the C values recovered from our data are 11, 45, and 16 respectively. This disagreement suggests that the strength of activity seen in the data is insufficient to explain the RV signal.

An alternative interpretation is that we are observing activity overlaid with a planet signal in the radial velocities. In this view, the correlation with activity indicator(s) in the RV residuals is independent of the Keplerian signal. One piece of evidence in favor of this interpretation comes from inspecting the correlation

plots before and after removal of the 3600-day Keplerian signal. If this signal is truly unrelated to the stellar activity, it should add random scatter about the correlation. Indeed, subtracting the Keplerian signal from the data reduces the scatter about the best-fit trend between RV and S_{HK} from 7.7 to 2.9 m s^{-1} and has a comparable effect on the correlations with other activity indices (Figure 3).

Inspecting the behavior of S_{HK} with time sheds some light on the evolution of HIP11915's activity level. As depicted in Figure 4, the stellar activity level exhibited an incoherent scatter until mid-2013, at which point it increased from the equivalent of $\log(R'_{HK}) \sim$ -4.87 to $\sim$ -4.82 by mid-2014. A concurrent rise in BIS and FWHM is also seen at this epoch. This level of variability is consistent with the behavior of the Sun, which has a mean $\log(R'_{HK})$ of -4.94 and an amplitude of variation around 0.1 dex over a full activity cycle (Hall et al. 2007). Given the recent increase in Ca emission, we could then expect a corresponding increase in short-duration activity phenomena such as spots and plages to manifest in the more recent RVs. This would add power to the correlations with line asymmetry indicators.

Ideally, we would be able to remove activity phenomena such as spots and plages by averaging our measurements over the timescale of the stellar rotation period, on the order of a month. Unfortunately the sampling of the data is too uneven to average effectively over the rotation period. We average instead over an entire observing season, which is a regime in which the time coverage should be distributed evenly enough to remove activity signals at periods shorter than a cycle. The resulting data from this seasonal binning trace the 3600-day signal well but show no statistically significant correlations with activity indicators.

In short, we have considered a variety of activity diagnostics and methods of cycle removal and the 3600-day signal remains robustly present in the data. The coincidence in phase between the rise in S_{HK} and the 3600-day signal maximum, however, calls for further monitoring of the star before we can definitively rule out the possibility of an activity cycle inducing the RV signal.

5. Summary

We have detected a Keplerian signal corresponding to a gas giant planet with a 10-year orbital period, consistent with a Jupiter twin, around the solar twin HIP11915. While we cannot conclusively exclude an activity cycle interpretation, commonly employed activity tracers fail to account for the signal. If the 3600-day signal is entirely induced by an activity cycle, the failure of various techniques to remove it bodes poorly for the prospect of correcting for such cycles in future long-period planet searches.

If this signal is truly planetary in origin, the HIP11915 system is a close analog to the solar system. Our analysis shows the planet HIP11915b to be a close match to Jupiter both in mass and orbital period, and its host star is extraordinarily similar to the Sun. Beyond having fundamental physical properties close to the Sun, initial spectroscopic analysis suggests that HIP11915 is also a solar twin in the sense of its detailed abundance pattern matching the solar pattern (Melendez et al. 2015, in prep). The presence of a Jupiter twin and a solar-like composition both make HIP11915 an excellent prospect for future terrestrial planet searches.
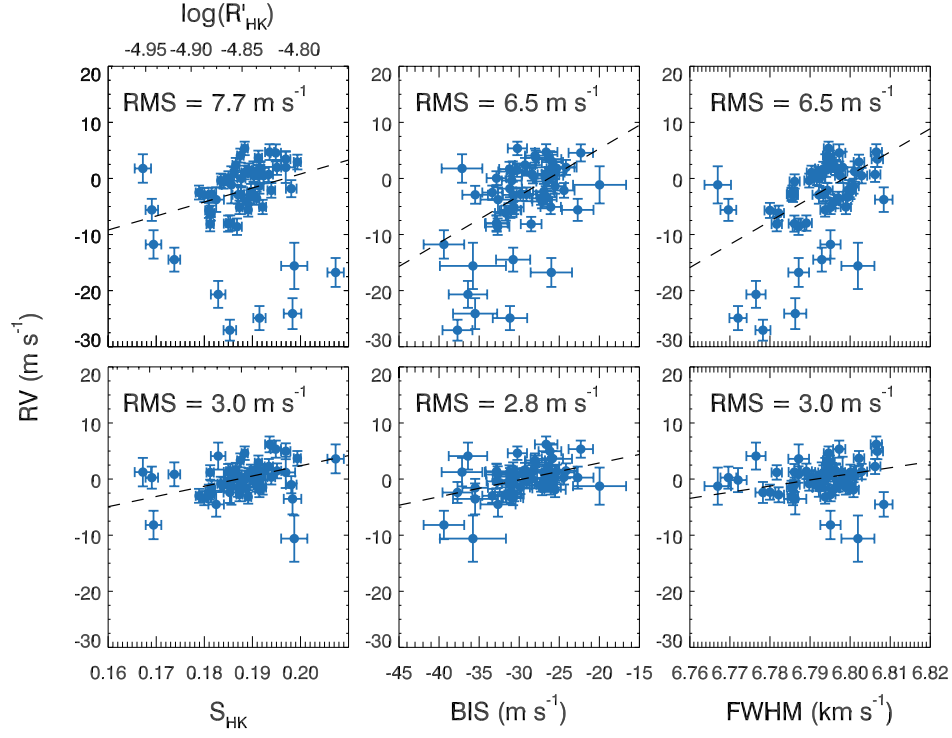
Fig. 3. Correlations for the activity tracers S_{HK}, BIS, and FWHM with radial velocity. The upper panels shows the observed RVs. The lower panels show the residuals to the 3600-day signal fit (as presented in Section 3.1). Dashed lines are linear least-squares best fits to the data.
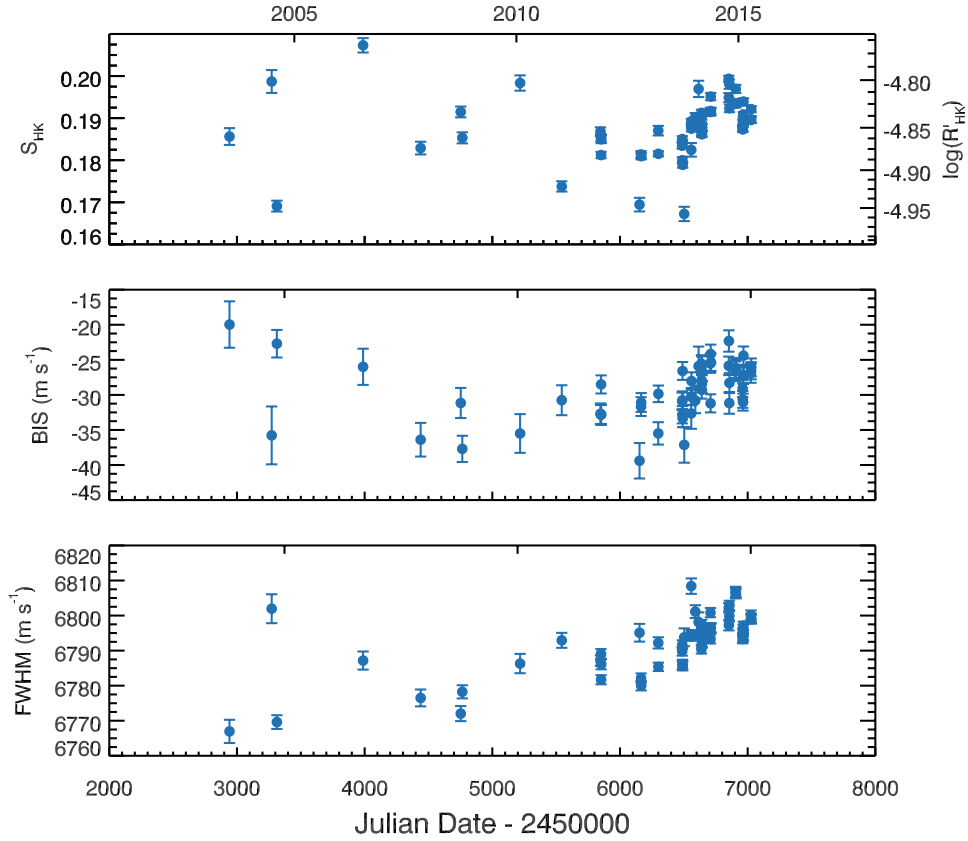

Fig. 4. Evolution of the activity indices S_{HK}, BIS, and FWHM with time. Errors on BIS and FWHM are approximated as the errors on the RVs.

References

Baliunas, S. L., Donahue, R. A., Soon, W. H., et al. 1995, ApJ, 438, 269
Bazot, M., Ireland, M. J., Huber, D., et al. 2011, A&A, 526, L4
Bedell, M., Meléndez, J., Bean, J. L., et al. 2014, ApJ, 795, 23
Boisse, I., Bouchy, F., Hébrard, G., et al. 2011, A&A, 528, A4
Boisse, I., Pepe, F., Perrier, C., et al. 2012, A&A, 545, A55
Dravins, D. 1985, in Stellar Radial Velocities, ed. A. G. D. Philip & D. W. Latham, 311–320
Dumusque, X., Lovis, C., Ségransan, D., et al. 2011, A&A, 535, A55
Feng, Y. K., Wright, J. T., Nelson, B., et al. 2015, ApJ accepted
Figueira, P., Santos, N. C., Pepe, F., Lovis, C., & Nardetto, N. 2013, A&A, 557, A93
Foreman-Mackey, D., Price-Whelan, A., Ryan, G., et al. 2014
Gelman, A. & Rubin, D. B. 1992, Statistical Science, 7, pp. 457
Hall, J. C., Lockwood, G. W., & Skiff, B. A. 2007, AJ, 133, 862
Howard, A. W., Johnson, J. A., Marcy, G. W., et al. 2010, ApJ, 721, 1467
Lovis, C., Dumusque, X., Santos, N. C., et al. 2011, ArXiv e-prints
Marmier, M., Ségransan, D., Udry, S., et al. 2013, A&A, 551, A90
Mayor, M., Pepe, F., Queloz, D., et al. 2003, The Messenger, 114, 20
Meléndez, J., Asplund, M., Gustafsson, B., & Yong, D. 2009, ApJ, 704, L66
Meunier, N. & Lagrange, A.-M. 2013, A&A, 551, A101
Naef, D., Mayor, M., Korzennik, S. G., et al. 2003, A&A, 410, 1051
Queloz, D., Bouchy, F., Moutou, C., et al. 2009, A&A, 506, 303
Queloz, D., Henry, G. W., Sivan, J. P., et al. 2001, A&A, 379, 279
Ramírez, I., Meléndez, J., & Asplund, M. 2009, A&A, 508, L17
Ramírez, I., Meléndez, J., Bean, J., et al. 2014, A&A, 572, A48
Saar, S. H. & Donahue, R. A. 1997, ApJ, 485, 319
Vogt, S. S., Marcy, G. W., Butler, R. P., & Apps, K. 2000, ApJ, 536, 902
Wittenmyer, R. A., Horner, J., Tinney, C. G., et al. 2014, ApJ, 783, 103
Wright, J. T. 2005, PASP, 117, 657
Wright, J. T., Marcy, G. W., Butler, R. P., et al. 2008, ApJ, 683, L63
Wright, J. T., Marcy, G. W., Fischer, D. A., et al. 2007, ApJ, 657, 533
Zechmeister, M. & Kürster, M. 2009, A&A, 496, 577
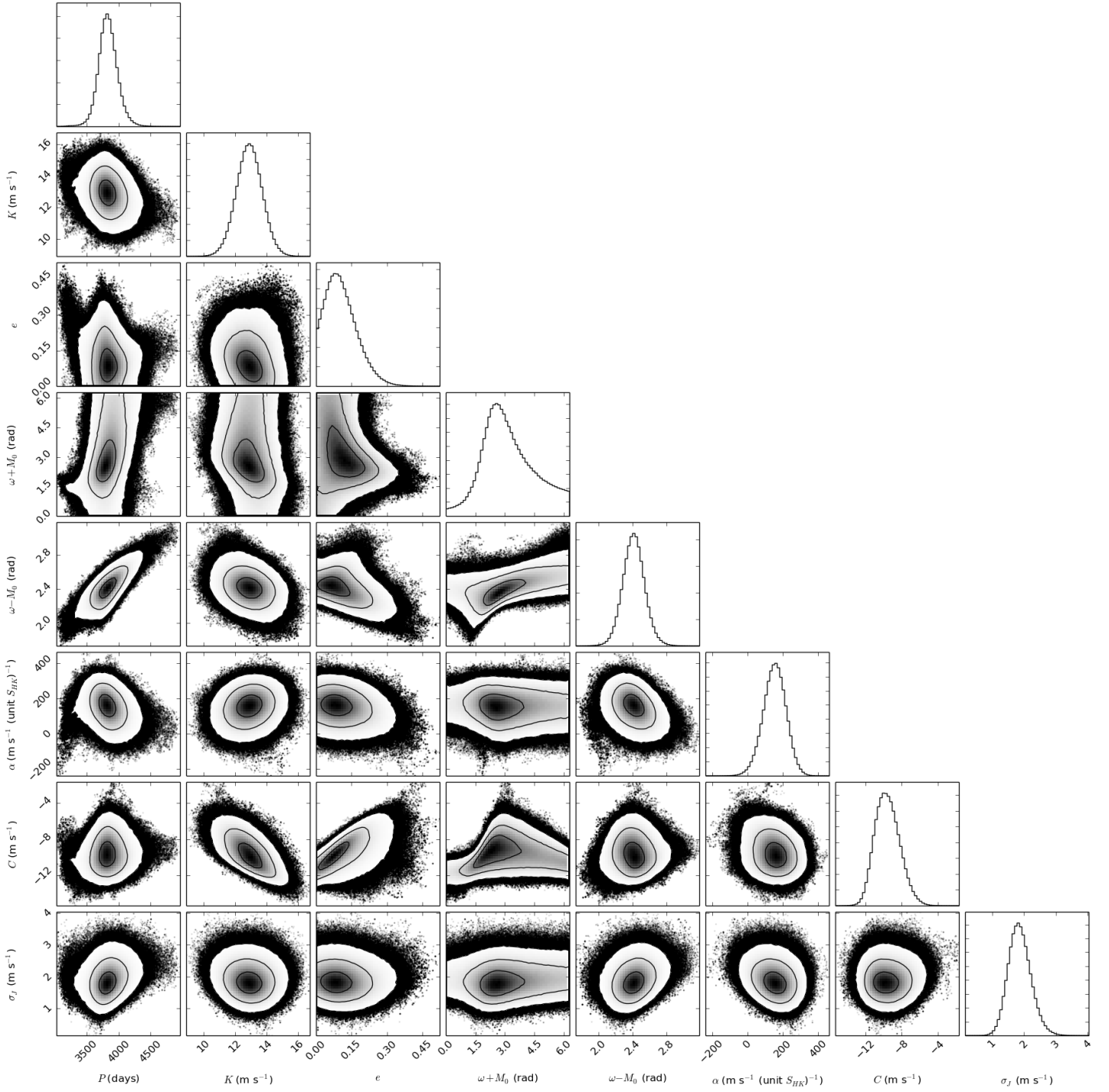Zechmeister, M., Kürster, M., Endl, M., et al. 2013, A&A, 552, A78

Fig. 5. Constraints on the fit to the radial velocities from the MCMC analysis. Parameters are defined in Section 3. Plot made using code from Foreman-Mackey et al. (2014).

Table 3. HARPS measured radial velocities and activity indices for HIP11915.

Julian Date	Exp. Time (s)	RV (km s^{-1})	σ_{RV} (km s^{-1})	S_{HK}	$\sigma_{S_{HK}}$	BIS (km s^{-1})	FWHM (km s^{-1})
2452941.7219	116.5	14.5766	0.0030	0.1856	0.0020	-0.0200	6.7670
2453271.8214	182.9	14.5622	0.0038	0.1987	0.0027	-0.0358	6.8019
2453312.6877	900.0	14.5722	0.0017	0.1691	0.0013	-0.0227	6.7696
2453987.7974	121.3	14.5610	0.0021	0.2073	0.0017	-0.0260	6.7872
2454438.6089	134.1	14.5571	0.0019	0.1829	0.0015	-0.0364	6.7765
2454752.7519	300.0	14.5529	0.0015	0.1915	0.0013	-0.0312	6.7720
2454764.7361	900.0	14.5507	0.0016	0.1853	0.0013	-0.0377	6.7782
2455217.5801	121.9	14.5537	0.0023	0.1983	0.0018	-0.0355	6.7863
2455543.6010	500.0	14.5633	0.0015	0.1738	0.0012	-0.0308	6.7929
2455846.8020	900.0	14.5692	0.0011	0.1868	0.0010	-0.0327	6.7871
2455850.7947	900.0	14.5698	0.0009	0.1854	0.0009	-0.0328	6.7891
2455851.7841	900.0	14.5697	0.0008	0.1812	0.0008	-0.0285	6.7817
2455852.7779	900.0	14.5697	0.0010	0.1850	0.0009	-0.0328	6.7861
2456152.8532	243.8	14.5660	0.0020	0.1694	0.0016	-0.0394	6.7951
2456164.9273	900.0	14.5716	0.0009	0.1814	0.0008	-0.0317	6.7822
2456165.9242	900.0	14.5721	0.0009	0.1810	0.0008	-0.0311	6.7800
2456299.6151	900.0	14.5749	0.0012	0.1870	0.0011	-0.0355	6.7922
2456300.5833	900.0	14.5750	0.0006	0.1815	0.0006	-0.0298	6.7854
2456486.9106	900.0	14.5774	0.0007	0.1834	0.0007	-0.0309	6.7898
2456487.8968	900.0	14.5778	0.0007	0.1850	0.0007	-0.0328	6.7917
2456488.9425	900.0	14.5749	0.0008	0.1800	0.0007	-0.0308	6.7857
2456489.9048	900.0	14.5773	0.0008	0.1840	0.0008	-0.0266	6.7862
2456490.8972	900.0	14.5753	0.0007	0.1789	0.0007	-0.0334	6.7856
2456502.9393	900.0	14.5796	0.0023	0.1672	0.0017	-0.0371	6.7938
2456557.9085	900.0	14.5740	0.0020	0.1825	0.0016	-0.0326	6.8084
2456558.8337	900.0	14.5793	0.0007	0.1892	0.0006	-0.0303	6.7940
2456559.8500	900.0	14.5819	0.0007	0.1875	0.0007	-0.0280	6.7945
2456560.8411	900.0	14.5831	0.0007	0.1884	0.0006	-0.0302	6.7946
2456589.8019	400.0	14.5790	0.0010	0.1902	0.0010	-0.0308	6.8011
2456615.6781	300.0	14.5798	0.0024	0.1969	0.0019	-0.0259	6.7981
2456637.6474	900.0	14.5789	0.0007	0.1884	0.0007	-0.0256	6.7904
2456638.6662	900.0	14.5815	0.0008	0.1913	0.0008	-0.0279	6.7949
2456639.6356	900.0	14.5802	0.0008	0.1866	0.0007	-0.0293	6.7955
2456640.6347	900.0	14.5783	0.0008	0.1904	0.0007	-0.0258	6.7975
2456641.6456	900.0	14.5786	0.0007	0.1862	0.0007	-0.0284	6.7921
2456643.6517	900.0	14.5778	0.0010	0.1877	0.0008	-0.0267	6.7923
2456708.5010	900.0	14.5764	0.0009	0.1915	0.0009	-0.0255	6.8008
2456709.5310	900.0	14.5795	0.0008	0.1917	0.0008	-0.0312	6.7933
2456710.5234	900.0	14.5798	0.0009	0.1951	0.0009	-0.0242	6.7964
2456711.5226	900.0	14.5796	0.0007	0.1916	0.0008	-0.0253	6.7965
2456851.9220	900.0	14.5807	0.0009	0.1993	0.0007	-0.0259	6.8022
2456852.8915	900.0	14.5823	0.0012	0.1949	0.0011	-0.0223	6.7973
2456855.8977	900.0	14.5760	0.0011	0.1981	0.0011	-0.0312	6.7999
2456856.8881	900.0	14.5783	0.0010	0.1923	0.0009	-0.0283	6.8029
2456904.8198	900.0	14.5825	0.0010	0.1936	0.0009	-0.0266	6.8065
2456906.7954	900.0	14.5812	0.0010	0.1969	0.0010	-0.0262	6.8068
2456907.8079	900.0	14.5785	0.0009	0.1934	0.0009	-0.0264	6.8062
2456960.7641	900.0	14.5750	0.0007	0.1876	0.0007	-0.0291	6.7933
2456961.7200	900.0	14.5726	0.0007	0.1873	0.0006	-0.0306	6.7951
2456963.7068	900.0	14.5722	0.0007	0.1891	0.0006	-0.0310	6.7938
2456964.7840	900.0	14.5737	0.0007	0.1887	0.0007	-0.0271	6.7961
2456965.6863	900.0	14.5743	0.0006	0.1909	0.0006	-0.0273	6.7971
2456966.7461	900.0	14.5757	0.0009	0.1939	0.0008	-0.0244	6.7943
2457025.5721	900.0	14.5755	0.0009	0.1897	0.0008	-0.0269	6.8001
2457026.6043	900.0	14.5745	0.0007	0.1896	0.0006	-0.0266	6.7993
2457027.5960	900.0	14.5727	0.0008	0.1921	0.0007	-0.0261	6.7989